Journal of Chromatography, 544 (1991) 319–344
Elsevier Science Publishers B.V., Amsterdam

CHROM. 22 945

Review

Microscopic characterization of high-performance liquid chromatographic packing materials

NOBUO TANAKA*, KAZUHIRO KIMATA and TAKEO ARAKI
Kyoto Institute of Technology, Department of Polymer Science and Engineering, Matsugasaki, Sakyo-ku, Kyoto 606 (Japan)
HAJIME TSUCHIYA
Nitto Technical Information Centre, Ibaraki, Osaka 567 (Japan)
and
KATSUSHI HASHIZUME
Tokuyama Soda, Co., Tokuyama 745 (Japan)

ABSTRACT

Transmission electron microscopic (TEM) studies on the internal structure of commercially available packing materials for high-performance liquid chromatography are reviewed. Clear micrographs are presented for wide-pore silica and polymer gels. TEM can provide straightforward information on the size, shape and location of pores and the skeleton in a particle. The results of densitometric measurements of TEM photographs are shown to visualize pore structures of wide-pore silica gels with the possibility of a three-dimensional representation.

CONTENTS

0021-9673/91/$03.50

INTRODUCTION

The characterization of pore structures of high-performance liquid chromatographic (HPLC) packing materials is important, as most chromatographic distribution processes take place in the pores of totally porous particles. Porous packing materials have customarily been subjected to characterization procedures such as measurement of surface area and pore size by nitrogen adsorption, mercury intrusion and size-exclusion chromatography (SEC). These methods, however, provide data only on the overall porosity and pore-size distribution of porous particles and do not give exact information about the shape or location of the pores.

A variety of structures have been suggested as the internal structures of porous materials [1,2]. The determination of physical parameters such as pore size and pore-size distribution depends on the shape of the pores [2,3].

Although scanning electron microscopy (SEM) is frequently used to show what the outer surface and fractured inner surface of packing materials look like, transmission electron microscopy (TEM) seems to give the most straightforward information regarding internal structures. There have been several reports on microscopic studies of the pore structures of chromatographic packing materials [4–14]. Tracz and Barna [12] reported the preparation of ultra-thin samples of porous materials for TEM by ion milling. Knox *et al.* [14] reported the internal structure of graphitized carbon packing materials.

In this paper our studies [15–17] on the TEM characterization of wide-pore HPLC packing materials will be summarized. Pore structures of commercially available wide-pore packing materials, including silica gels, porous glass particles and macroporous polymer gels, will be visualized. Clear internal structures obtained by TEM show whether the packing materials actually possess the stated pore size and uniformity, and can give information on how the particles were prepared. The understanding of results obtained, *e.g.*, by reversed-phase liquid chromatography (RPLC), SEC and nitrogen adsorption measurements, will be much easier if one knows the internal structures of the HPLC packing materials involved.

2. INTERNAL STRUCTURES OF GLASS AND SILICA PARTICLES

The packing materials listed in Table 1 were subjected to TEM observation by making ultra-thin sections of about 80 nm thickness. Porous particles were first embedded in epoxy resin, then hardened before the preparation of ultra-thin sections with a Sorvall MT-6000 ultramicrotome (DuPont). Polymer gels having polar functionality were stained with ruthenium tetraoxide vapour prior to epoxy resin impregnation. Electron microscopy was carried out at the Nitto Technical Information Centre by using an H-800 electron microscope (Hitachi). Nitrogen adsorption measurements were carried out at the Shiseido Research Centre.

Clear electron micrographs of pore structures were obtained for wide-pore packing materials. In these transmission electron micrographs, the ligth areas represent the epoxy resin in the pores and in the interparticle space and the dark areas the skeleton. The loss of a part of the ultra-thin section resulted in extremely light areas.

Fig. 1a and b clearly demonstrate the differences in pore structure between a porous glass particle and a wide-pore silica gel, LiChrospher Si 500. Whereas the

TABLE 1

PORE PARAMETERS OF WIDE-PORE PACKING MATERIALS

Manufacturer's specifications (values found experimentally by nitrogen adsorption are given in parentheses).

Packing material	Surface area (m^2/g)	Pore size (nm)[a]	Pore volume (ml/g)	Particle size (μm)
LiChrospher Si 500	50(69)	50(40)	0.8(0.90)	10
Si 1000	20	100	0.8	10
Si 4000	6	400	0.8	10
Nucleosil 300	100(109)	30(15,70)	0.8(0.81)	5
1000	25	100	0.8	5
4000	10	400	0.7	5
Hypersil 300	60(58)	30(20)	0.6(0.53)	5
500E[b]	(70)	50(40)	(1.24)	5
Spherisorb 300	190(209)	30(35)	1.5(1.62)	5
Vydac TP	80(93)	30(26)	0.6(0.69)	10
Porous glass	(386)	(55)	(0.72,0.49[c])	10
TSK G4000H	(333)	–	1.29(1.19)	12
TSK G4000PW	(64)	(50)	(0.64)	10
Asahipak ODP-50	(108)	(26)	(0.57)	6
PLRP-S 300	(380)	30(60)	(1.26)	8
Shodex DE-613	(354)	(5)	(0.41)	6
Shodex D4-613	(100)	–	(0.54)	6

[a] Experimental values indicate the pore diameter corresponding to the maximum in the pore volume–pore radius plot.
[b] Experimental batch.
[c] Mercury porosimetry.

pores in the glass particles are round and relatively uniform in size, those in LiChrospher Si 500 are irregularly shaped and possessed a broad size distribution. The glass particles seem to possess a spongy system, solids having channels, whereas the silica particles possess a corpuscular system, agglomerates of microstructures.

Fig. 2 shows the densitograms obtained from the photographs in Fig. 1 for the glass particle and LiChrospher Si 500 (B) by scanning the photographs shown in Fig. 1a and b using a CS 9000 Chromatoscanner (Shimadzu) with a beam size 0.4 mm × 0.4 mm. The horizontal axis corresponds to the distance, total 2 μm in these instances, on the ultra-thin sections shown in Fig. 1, and the vertical axis corresponds to the darkness of the photograph which in turn is related to the thickness of the material, total *ca.* 80 nm in these instances. The magnitude of the vertical axis, expanded about ten times compared with the horizontal axis in Fig. 2, could be strongly dependent on how the photographs were prepared. The results, however, reflected an almost constant thickness of skeleton, and gave a clear differentiation between the pores and the skeletons when the pores were sufficiently large.

In a porous glass particle, many pores reach directly to the bottom of the section with relatively even spacing, indicating the wide channels in solids, while only a few straight pores reach to the bottom of the section with LiChrospher Si 500. The

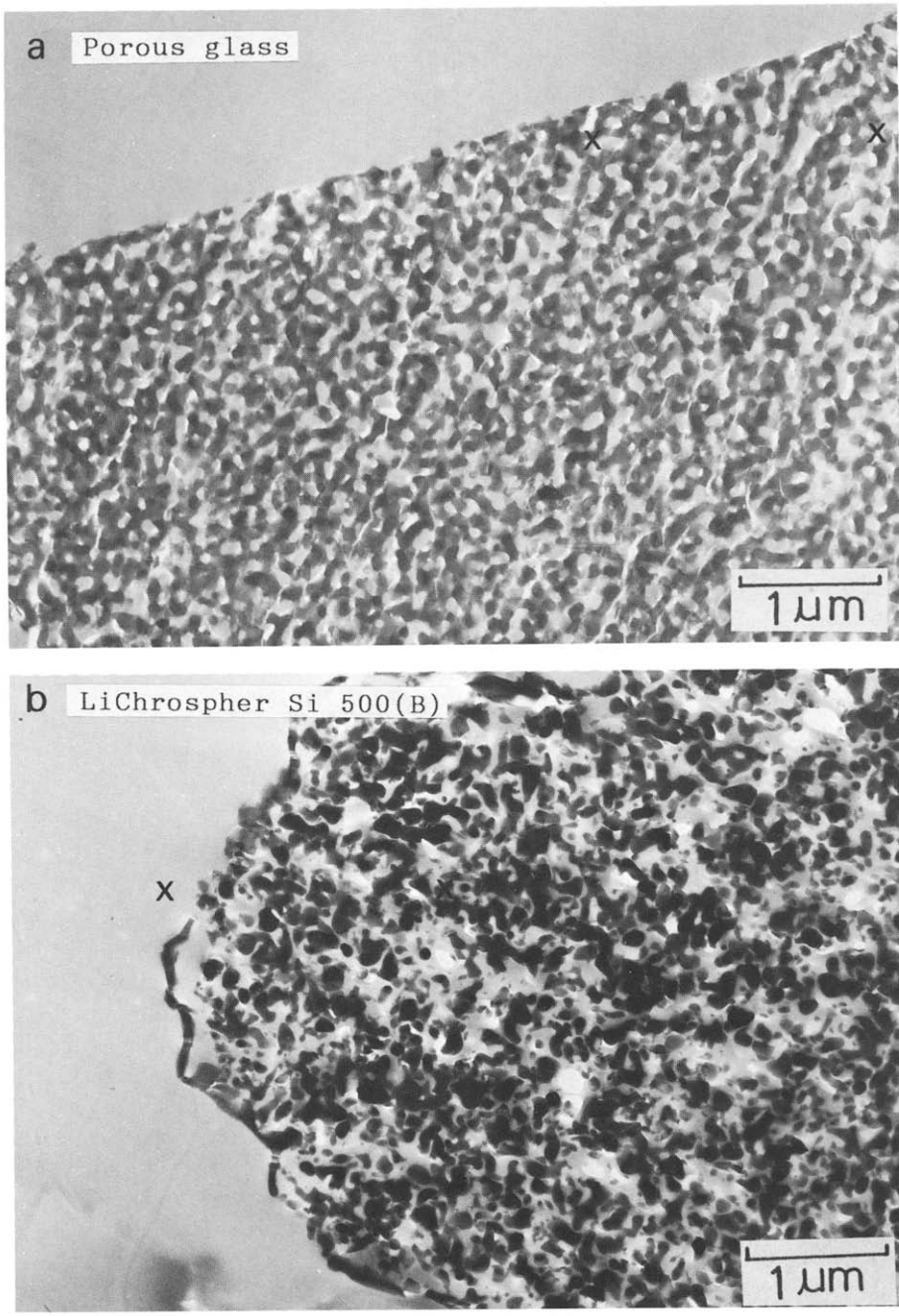

Fig. 1.

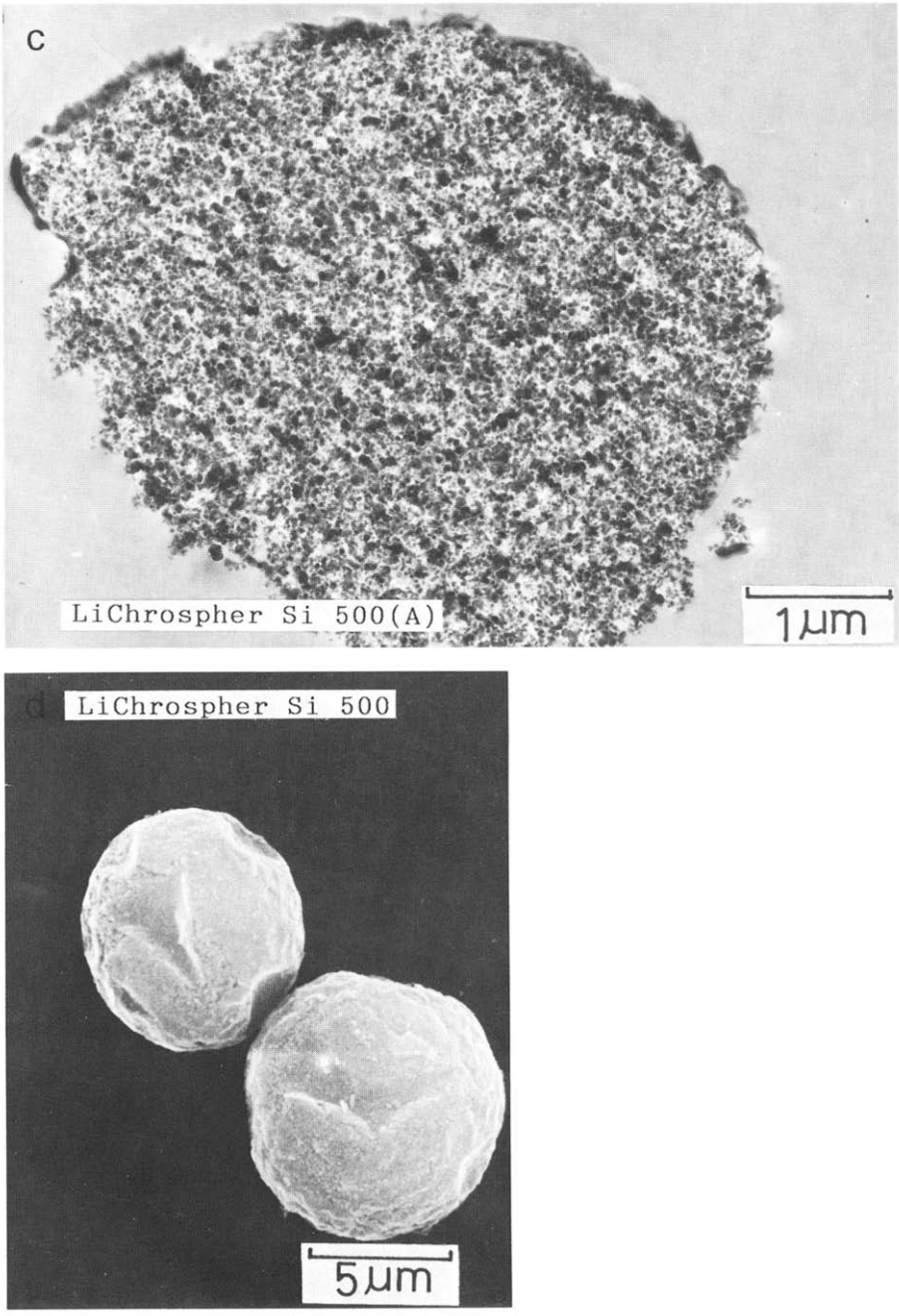

Fig. 1. TEM photographs of (a) porous glass and (b and c) LiChrospher Si 500 and (d) SEM photograph of LiChrospher Si 500.

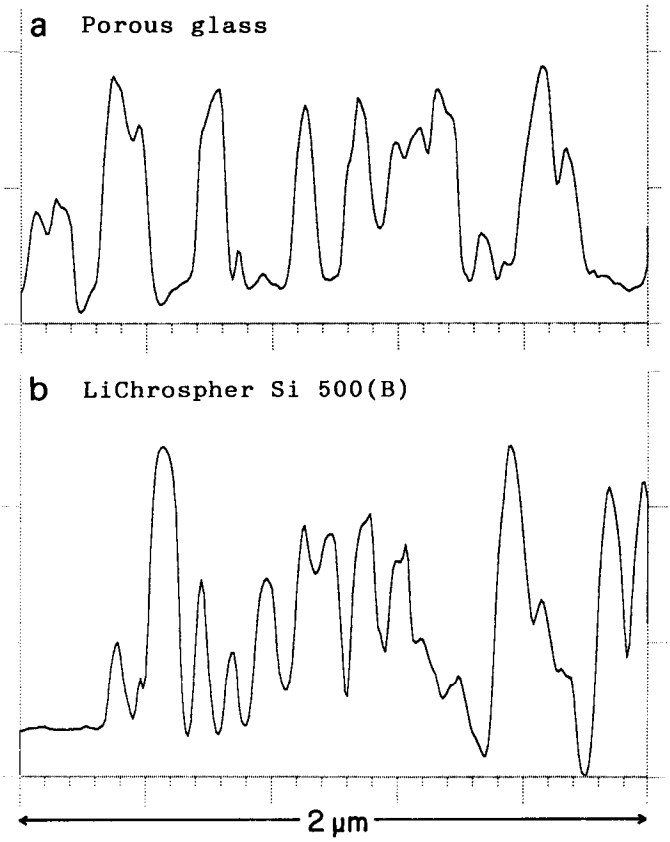

Fig. 2. Pore structures of (a) porous glass particle and (b) LiChrospher Si 500B silica particle expressed as densitograms which were obtained by scanning the TEM photographs in Fig. 1a and b, respectively, along the line connecting the two Xs. Direction of scan, Fig. 1a, from right to left; Fig. 1b, from left to right. The vertical scale is expanded about ten times compared with the horizontal scale. The thickness of the section is *ca.* 80 nm.

latter structure is compatible with a corpuscular system, indicating that the channels are the interstices of agglomerates of spheres. Hence the densitograms of TEM photographs may provide information on the regularity of pore structures and on how the pores penetrate the section, depending on the thickness of the section and the pore size. Further examination of densitograms from TEM photographs will be given later in an attempt to visualize the pore structures.

Interestingly, the LiChrospher Si 500 packing material contained two types of particles shown in Fig. 1b and c. The pore size of LiChrospher Si 500 (A) is much smaller than that of LiChrospher Si 500 (B). The difference, however, cannot readily be seen by SEM owing to the presence of shells around the particles, as shown in Fig. 1d, unless the shells are removed by ultrasonication. All LiChrospher particles possessed shells outside the spheres, which seem to have been produced by heat treatment

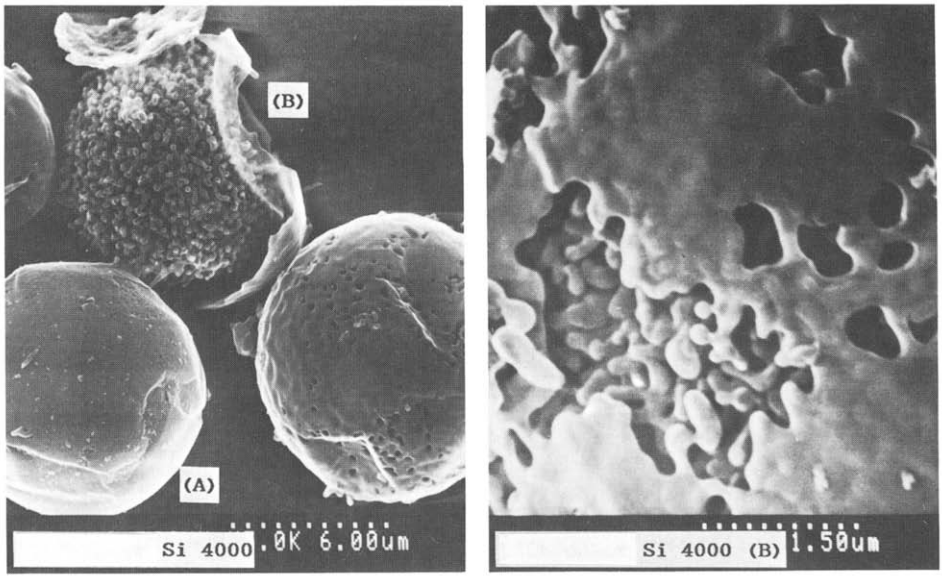

Fig. 3. SEM photographs of LiChrospher Si 4000.

after the formation of spheres, from the appearance of the sintered structure shown in Fig. 3.

The surface shells on highly porous materials are relatively fragile, as was also pointed out by Unger and Gimpel [18]. Prolonged ultrasonication of these particles should be avoided prior to column packing.

3. PRESENCE OF MORE THAN ONE TYPE OF PARTICLE IN A BATCH OF SILICA GEL

3.1. Wide-pore LiChrospher particles

Fig. 1b and c were obtained from a single batch of LiChrospher Si 500. The internal structures of these silica particles are evidently different. One type of particle possesses a pore diameter of less than 30 nm and the other up to 300 nm. Both types of particles are covered with a shell which produced a dark area at the periphery of the spheres. No particles having intermediate pore structures were observed in an ultra-thin section containing more than 20 particles.

According to several manufacturers, more than one type of internal structure can be made in a batch of silica gel owing to the inhomogeneity of the reaction conditions in a controlled sintering process [2]. In fact the existence of pore structures of precursors in the enlarged pores of final products can be seen in some of the following figures.

Although it is not clear whether the particles were intentionally blended, possibly to obtain a pore-size distribution and surface area within certain specifications, the particles containing more than one type of particle will be called "blended" in this paper. Some packing materials having a pore size of 30 50 nm and most of those with pore sizes of 100 and 400 nm currently available are blended particles. These packing

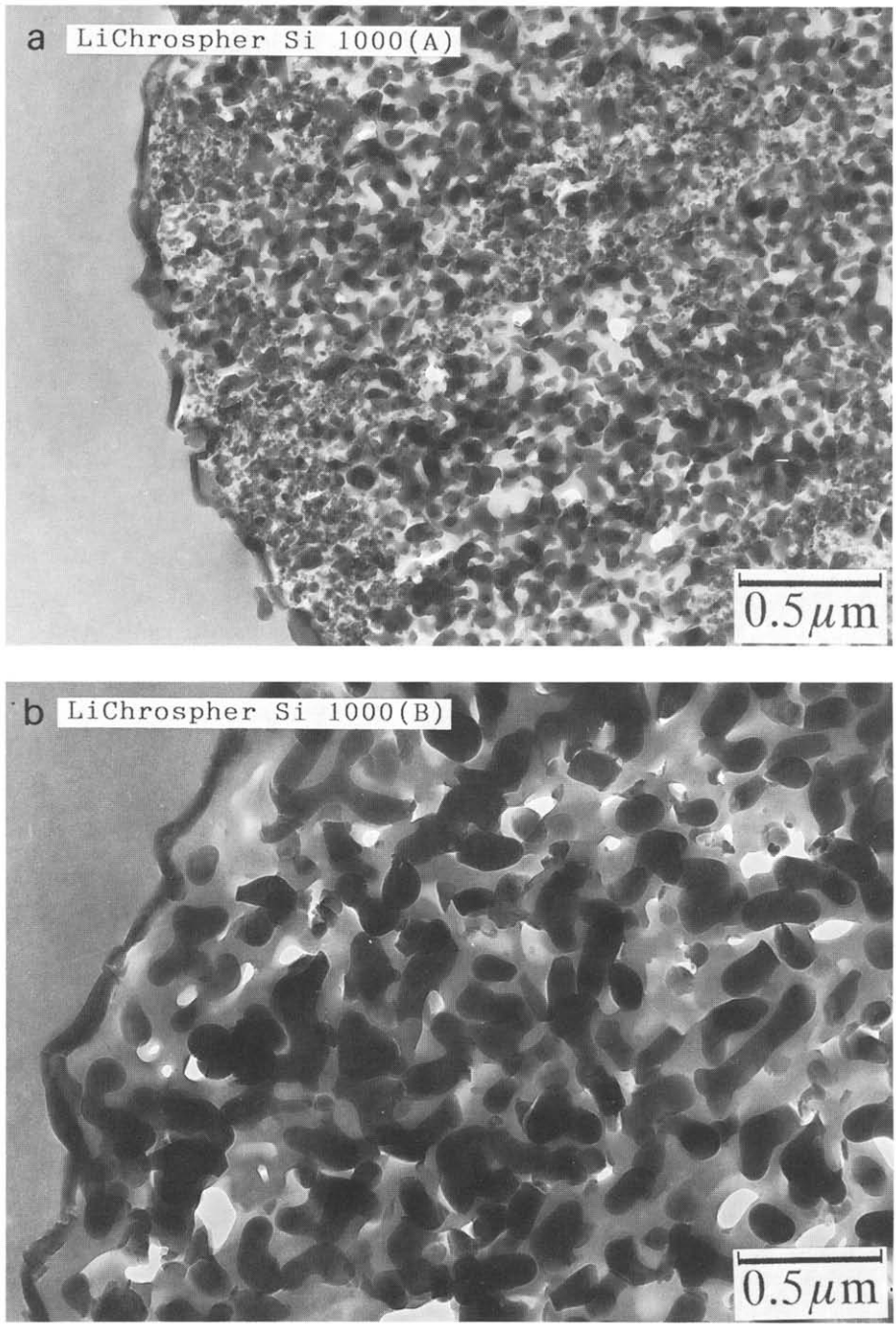

Fig. 4. TEM photographs of LiChrospher Si 1000.

materials generally showed excellent performance for the separation of high-molecular-weight polypeptides [16,17].

Fig. 4 shows the two types of particles having different pore sizes found in LiChrospher Si 1000. One type possesses pores of 50–100 nm and the other pores up to 200 nm. One type, LiChrospher Si 1000A in Fig. 4a, shows the existence of portions having a much smaller pore size. This seems to be an indication of a controlled sintering process in the preparation of this material, starting from particles with much smaller pore sizes. Particle B possesses a very similar internal structure as found in one type of particle in LiChrospher Si 4000.

Fig. 5 shows that LiChrospher Si 4000 also consists of two types of silica; one type (A) is similar to LiChrospher Si 1000(B) and the other has much higher porosity. The latter possesses some crystallinity in the silica skeleton, as shown by the moiré pattern. The crystallinity was lost during the TEM observation, presumably owing to the heat. The pore structures of these silica particles are similar to that in a spongy system. As mentioned by Unger [2], silica particles can have a spongy structure depending on the method of preparation.

3.2. Wide-pore Nucleosil particles

Although it is not possible to observe the internal structures of LiChrospher particles by SEM owing to the presence of surface shells, the difference in the internal structures in Nucleosil particles can be observed by SEM, as shown in Fig. 6a.

At least three types of particles having different surface roughness constitute Nucleosil 300. About 10% of the particles (C in Fig. 6a) possess a rough surface with a pore size of 100–200 nm. A microstructure, presumably a precursor of this silica, was found in some of Nucleosil 300(C) particles. The other two types of particles possess much more compact structures with pore sizes smaller than 30 nm. The particle A possesses much smaller structural units, but not as small as Nucleosil 100 shown in Fig. 7. Particles with smaller pores possess a typical corpuscular structure, while particles with larger pores possess a spongy structure, as is the case with LiChrospher particles.

Nucleosil 1000 and Nucleosil 4000 were also found to be mixtures of two or more types of silicas, as shown in Figs. 8 and 9. Nucleosil 1000 contained one type of particles (A) that were more compact than the other (B), which possess a pore size of about 200 nm.

Nucleosil 4000 contained three major constituents in comparable amounts, as seen in Fig. 9a. Two of them (A and B) are similar to those present in Nucleosil 300 and 1000. Particle C, with pores up to 500 nm, shows the development of a crystalline structure in the silica skeleton and the surface shell, similarly to LiChrospher Si 4000 (B) in Fig. 5. A very few particles with a smooth surface (D in Fig. 9a) were also found in Nucleosil 4000.

4. UNBLENDED WIDE-PORE SILICA GELS

There are several unblended wide-pore silica particles commercially available. No evidence of blending was seen with Hypersil 300, Spherisorb 300 and Vydac TP or with an experimental batch of Hypersil 500 by observing at least 20–30 particles in the ultra-thin sections. All the particles possess typical corpuscular structures, with some

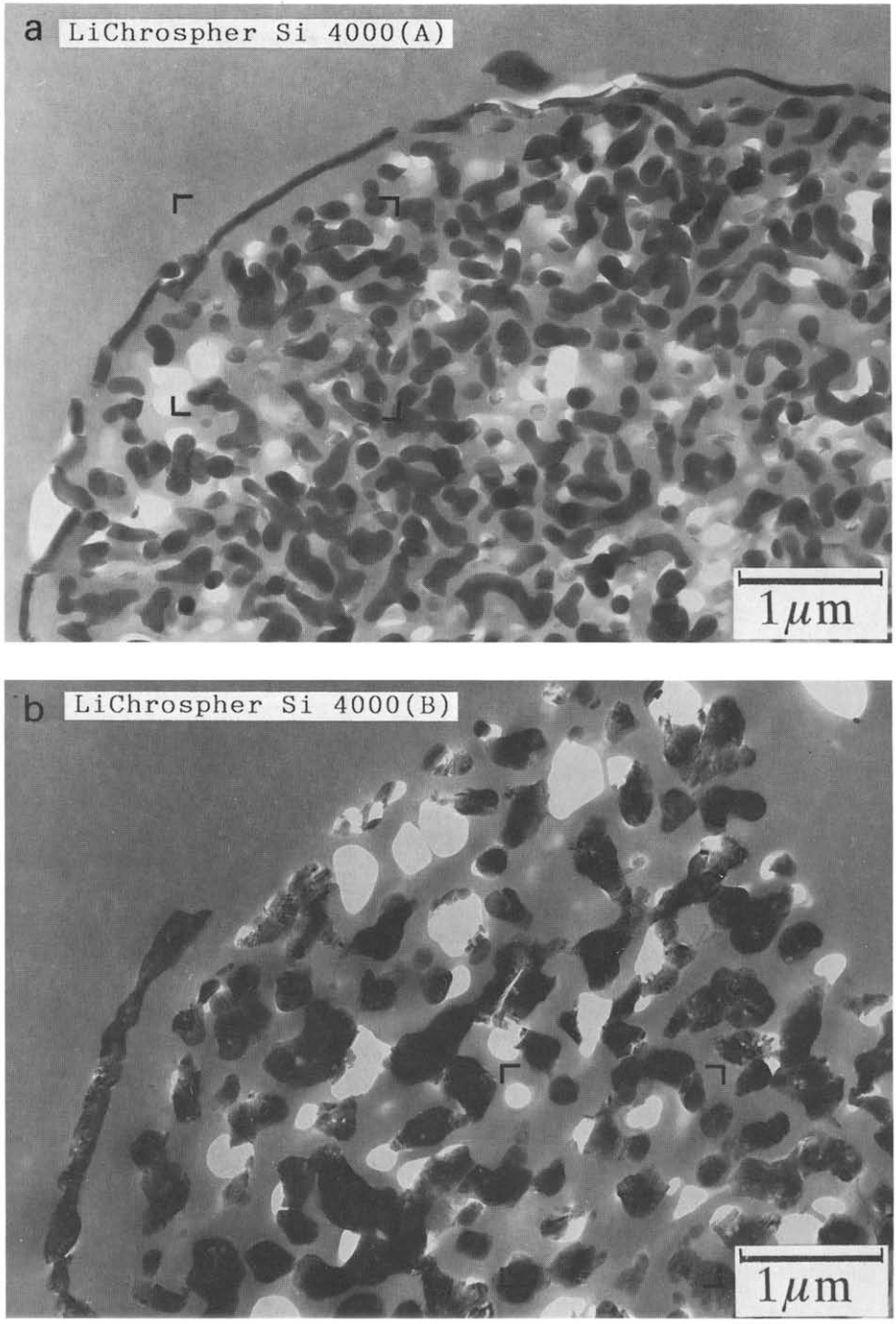

Fig. 5. TEM photographs of LiChrospher Si 4000.

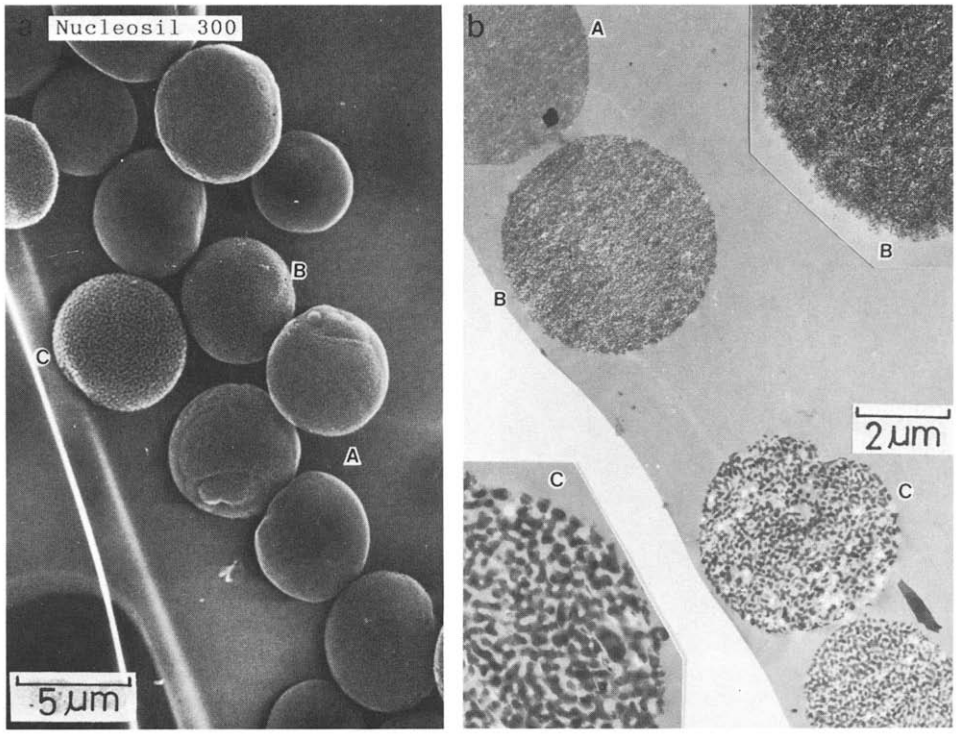

Fig. 6. (a) SEM photograph and (b) TEM photograph of Nucleosil 300. Particles B and C are enlarged 2.5 times in the insets.

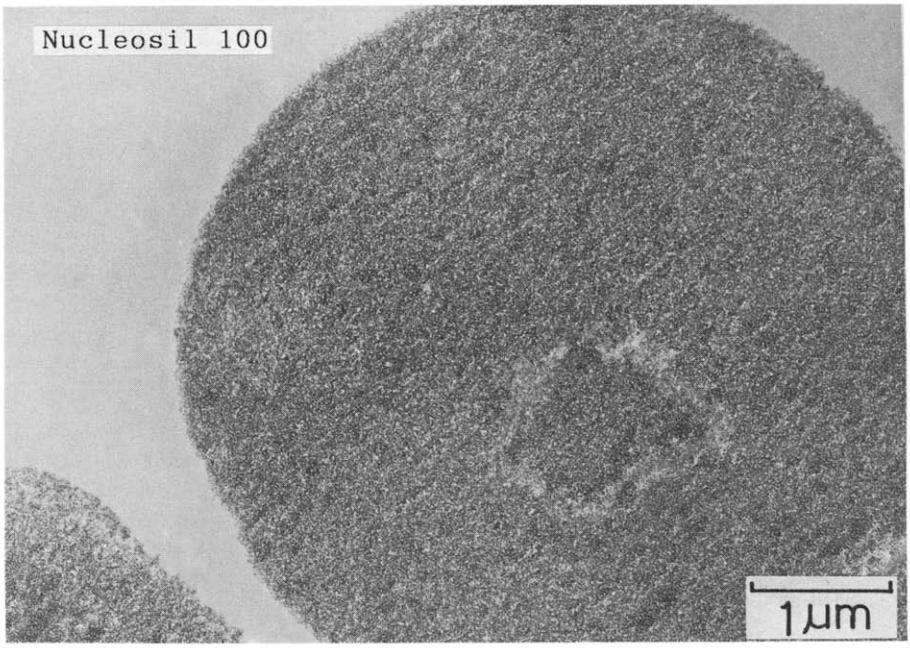

Fig. 7. TEM photograph of Nucleosil 100.

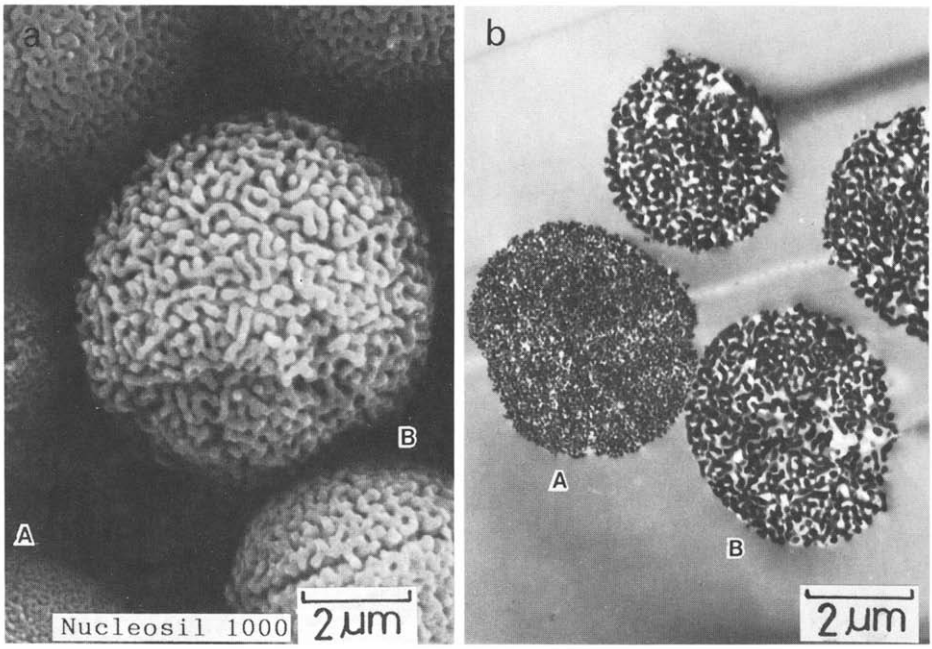

Fig. 8. (a) SEM and (b) TEM photographs of Nucleosil 1000.

irregularities in the case of Vydac, as pointed out by Kohler and Kirkland [19] from SEM observation.

Fig. 10b shows the highly porous structure of Spherisorb 300, which possesses an unusually high surface area and large pore volume for a wide-pore silica. The

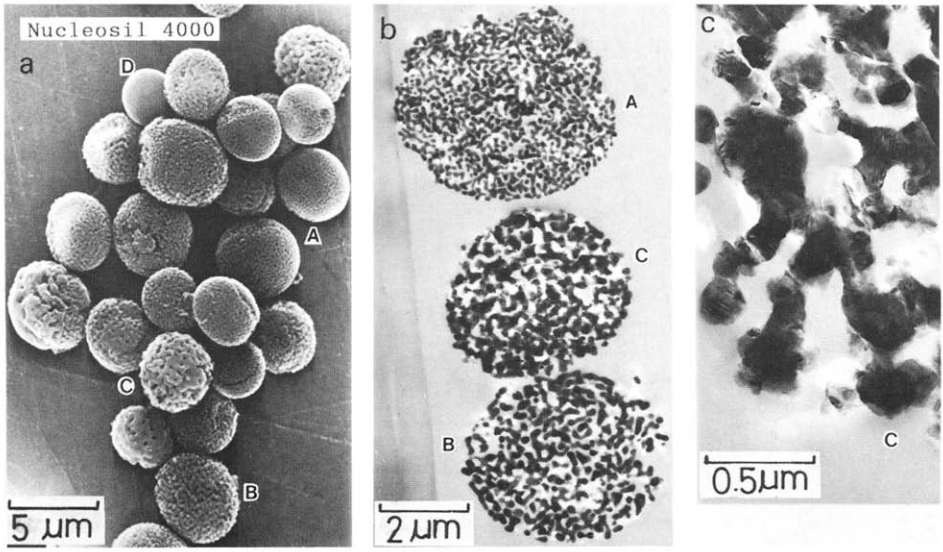

Fig. 9. (a) SEM and (b and c) TEM photographs of Nucleosil 4000.

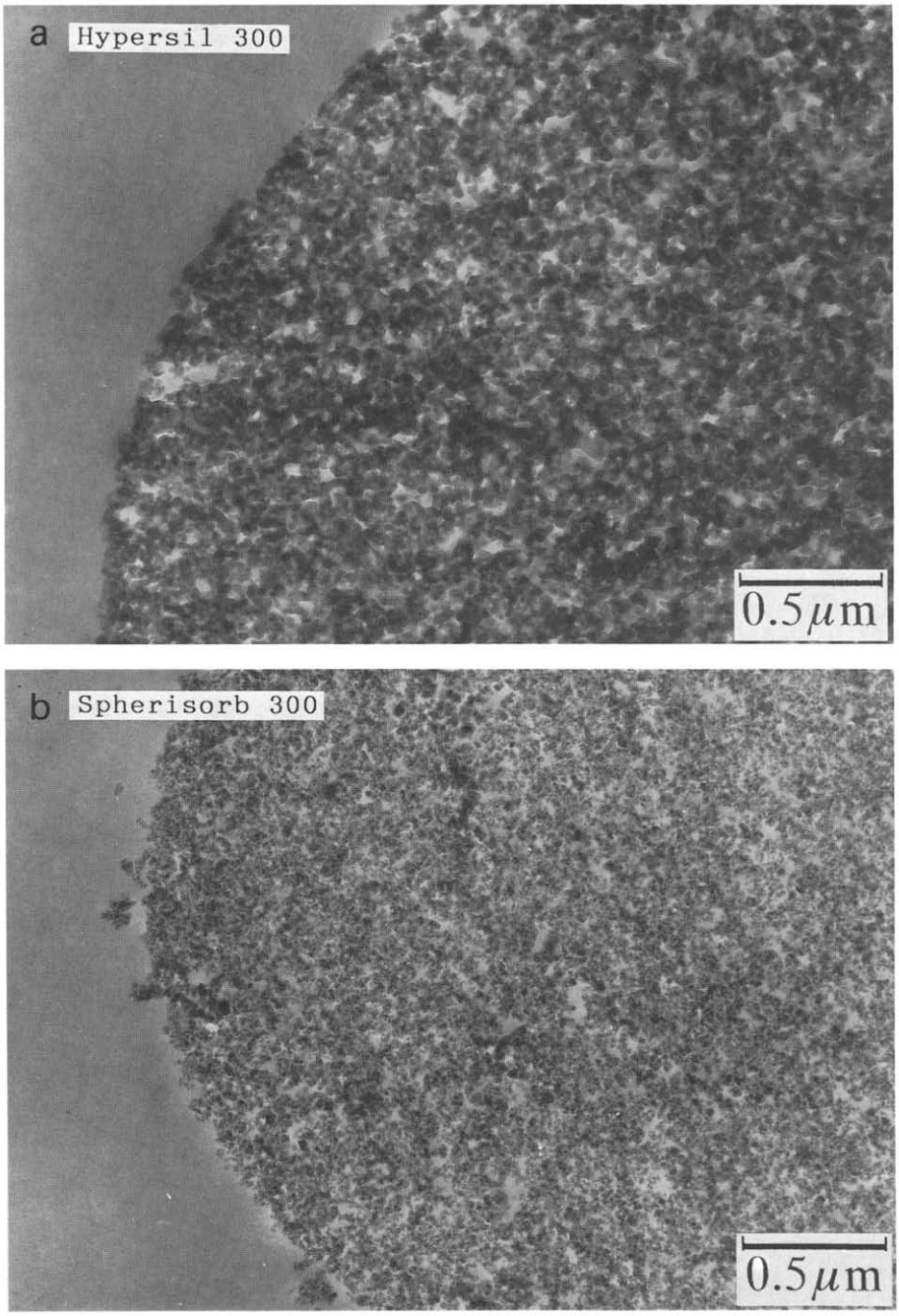

Fig. 10.

(Continued on p. 332

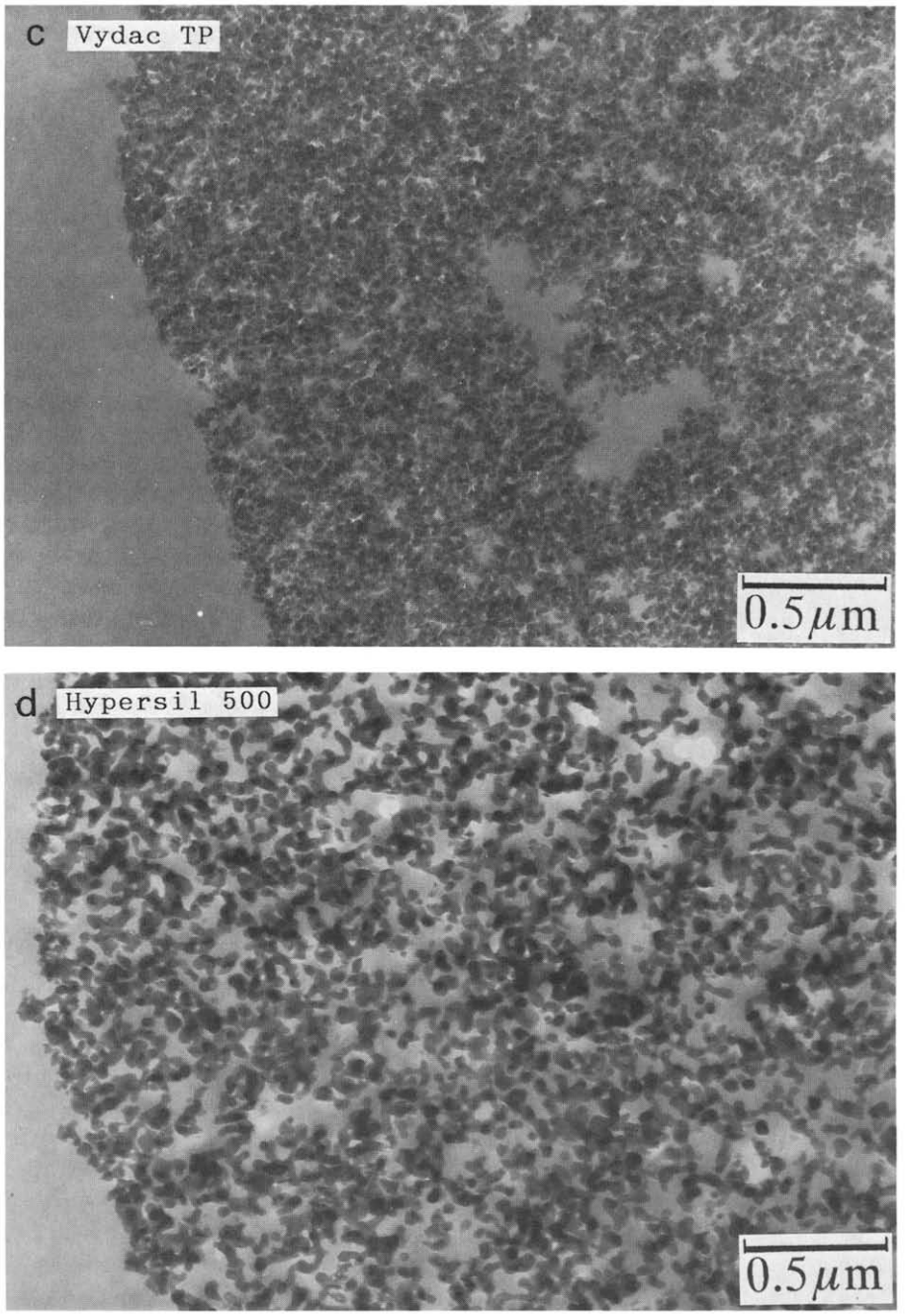

Fig. 10. TEM photographs of (a) Hypersil 300, (b) Spherisorb 300, (c) Vydac TP and (d) Hypersil 500E.

primary structural units in Hypersil 300 and Vydac TP have larger dimensions than those in Spherisorb 300, showing a more compact structure with a thick skeleton. The difference is clearly seen in the densitograms in Fig. 11. The porosities of Hypersil 300

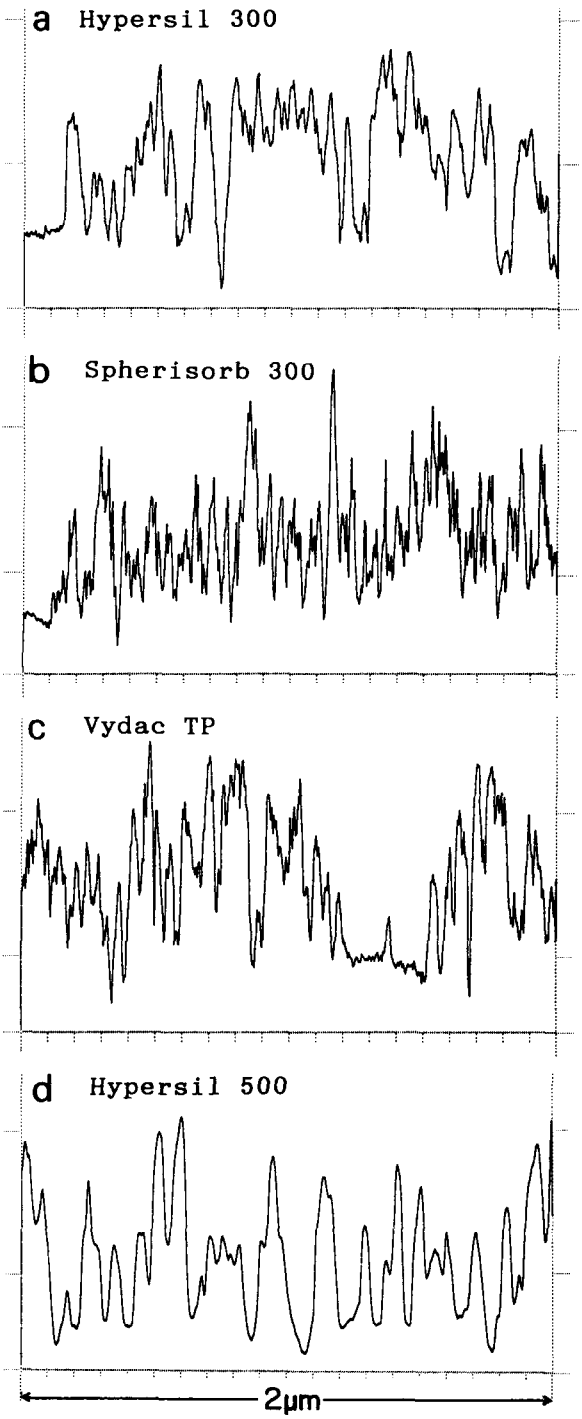

Fig. 11. Pore structures of (a) Hypersil 300, (b) Spherisorb 300, (c) Vydac TP and (d) Hypersil 500E expressed as densitograms which were obtained from the TEM photographs in Fig. 10. The vertical scale is expanded about ten times compared with the horizontal scale. The thickness of the section is *ca.* 80 nm.

and Vydac TP, except for the large irregular pores in the latter, are much lower than that of Spherisorb, in spite of the similar specifications of 30-nm pores. Many pores penetrate the total thickness of the section with Spherisorb 300, in contrast to only a few on Hypersil 300 and Vydac TP.

RPLC packing materials based on highly porous particles such as LiChrospher Si 500 and Spherisorb 300 showed a better performance for high-molecular-weight polypeptides than those derived from particles with more compact structures [16,17]. Hypersil 500E possesses a highly porous structure with a relatively thick skeleton compared with Spherisorb 300.

5. TRANSMISSION ELECTRON MICROGRAPHS OF POLYMER GELS

Figs. 12 and 13 show the SEM and TEM photographs for TSK G4000H, a poly(styrene–divinylbenzene) gel, and TSK G4000PW, a poly(hydroxyalkyl acrylate or methacrylate) gel. Fig. 14 shows the TEM photographs of polymer-based RPLC packing materials that recently became available. Whereas PLRP-S 300 is a poly (styrene–divinylbenzene) gel, Asahipak ODP-50, octadecanoylated poly(vinyl alcohol), Shodex DE-613, poly(alkyl methacrylate), and Shodex D4-613, poly(hydroxyalkyl methacrylate) butyl ether, are alkyl-type gels. Ruthenium tetraoxide staining was needed to prevent the disintegration of the particles in these alkyl-type gels.

All the polymer gel particles are aggregates of microspheres, a typical corpuscular system, whereas TSK G4000PW particles possess the features of a spongy system. Most polymer gels are totally macroporous, possessing pores in a range of 30–50 nm

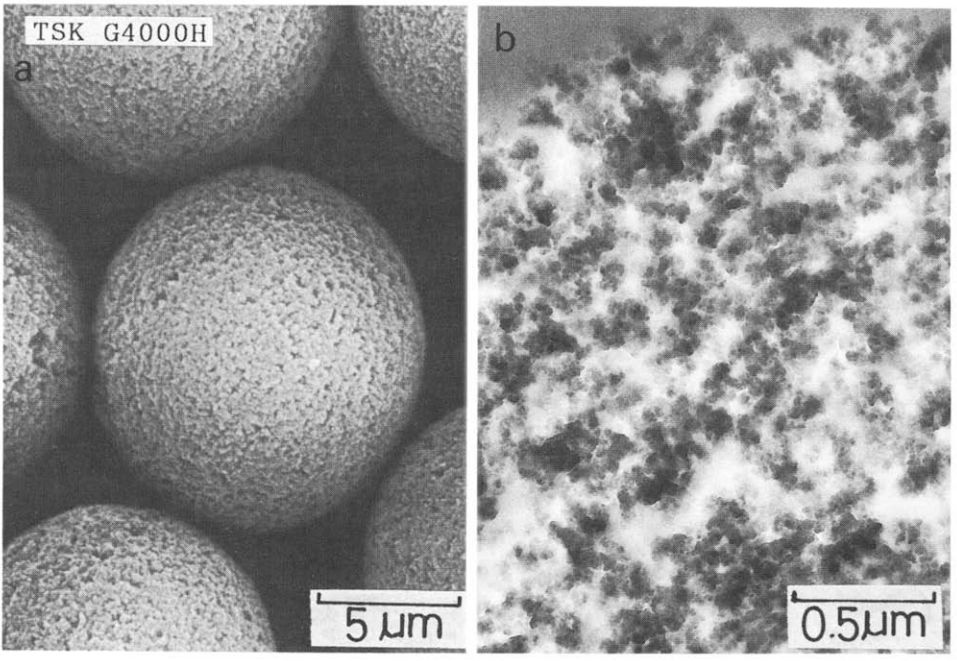

Fig. 12. (a) SEM and (b) TEM photographs of TSK G4000H.

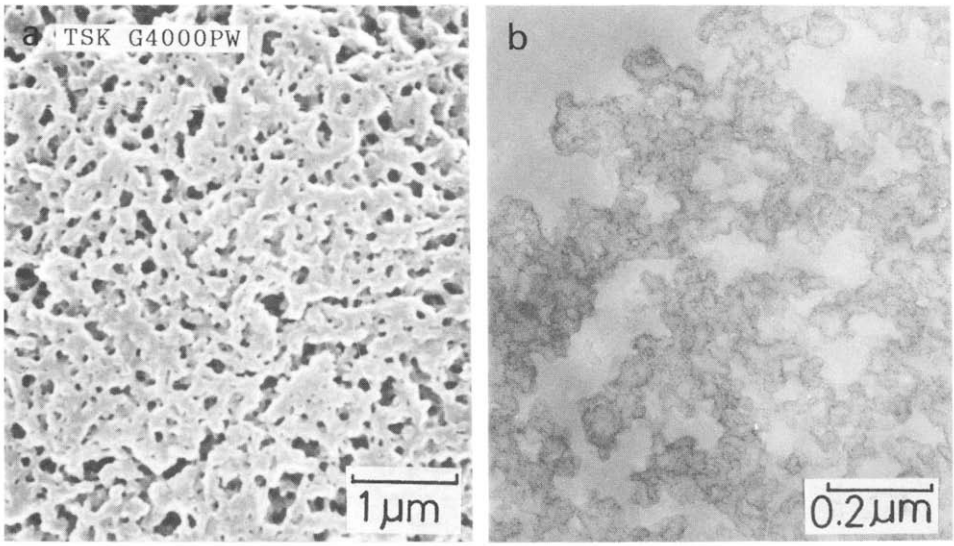

Fig. 13. (a) SEM and (b) TEM photographs of TSK G4000PW.

or greater, and Shodex DE 613 possesses a porous region only at the periphery of the particles. All the polymer gels showed broad and bimodal pore-size distributions with abundant micropores [16,17].

The TEM photographs cannot account for the bimodal pore-size distribution for polymer gels found in nitrogen adsorption and inverse SEC. The presence of a biporous structure of polymer gels [20,21], macroporous particles consisting of microporous primary structures, resulted in selective binding of small molecules relative to high-molecular-weight compounds, especially for rigid, planar aromatic compounds in RPLC [21–23]. The micropores responsible for the steric selectivity cannot be seen by TEM at this magnification. At higher magnification, the gel structures are much less stable. The presence of micropores that can trap organic molecules seems to provide unique selectivity and performance of polymer gels different from those of a silica C_{18} phase [21–25].

Recent chromatographic studies of polymer-based packing materials, including Asahipak ODP, PLRP-S 300, Shodex DE-613 and Shodex D4-613, showed that the location of pores in the particle is important when these packing materials are applied to the separation of high-molecular-weight polypeptides.

All polymer gels having macropores over the entire particle showed excellent performance for polypeptides with molecular weights up to 80 000, whereas that with a superficial macroporous region showed limited performance for polypeptides in spite of its excellent performance for small molecules [22]. TEM photographs of polymer gels having very large pores of up to 1–2 μm have been presented recently [26].

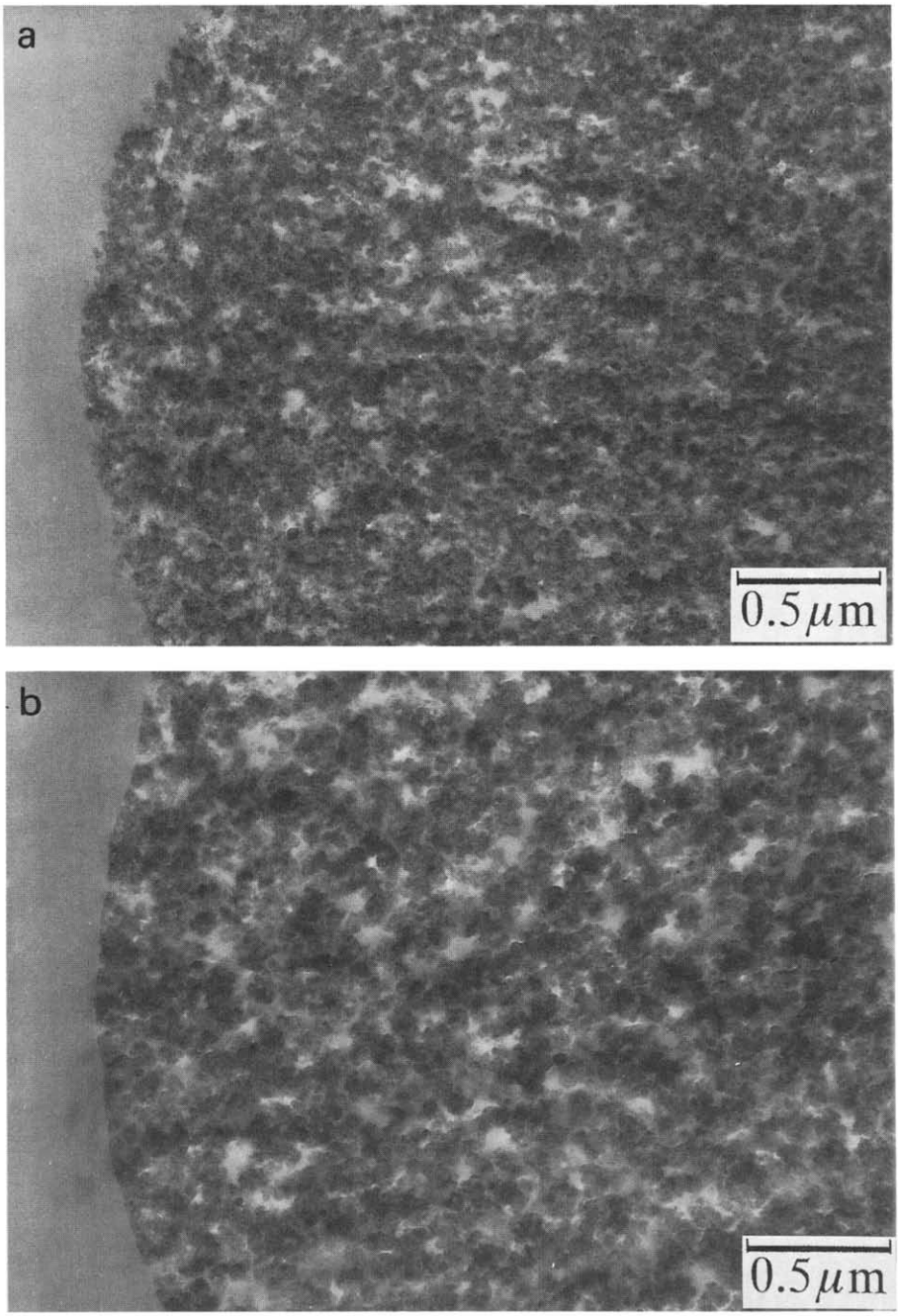

Fig. 14.

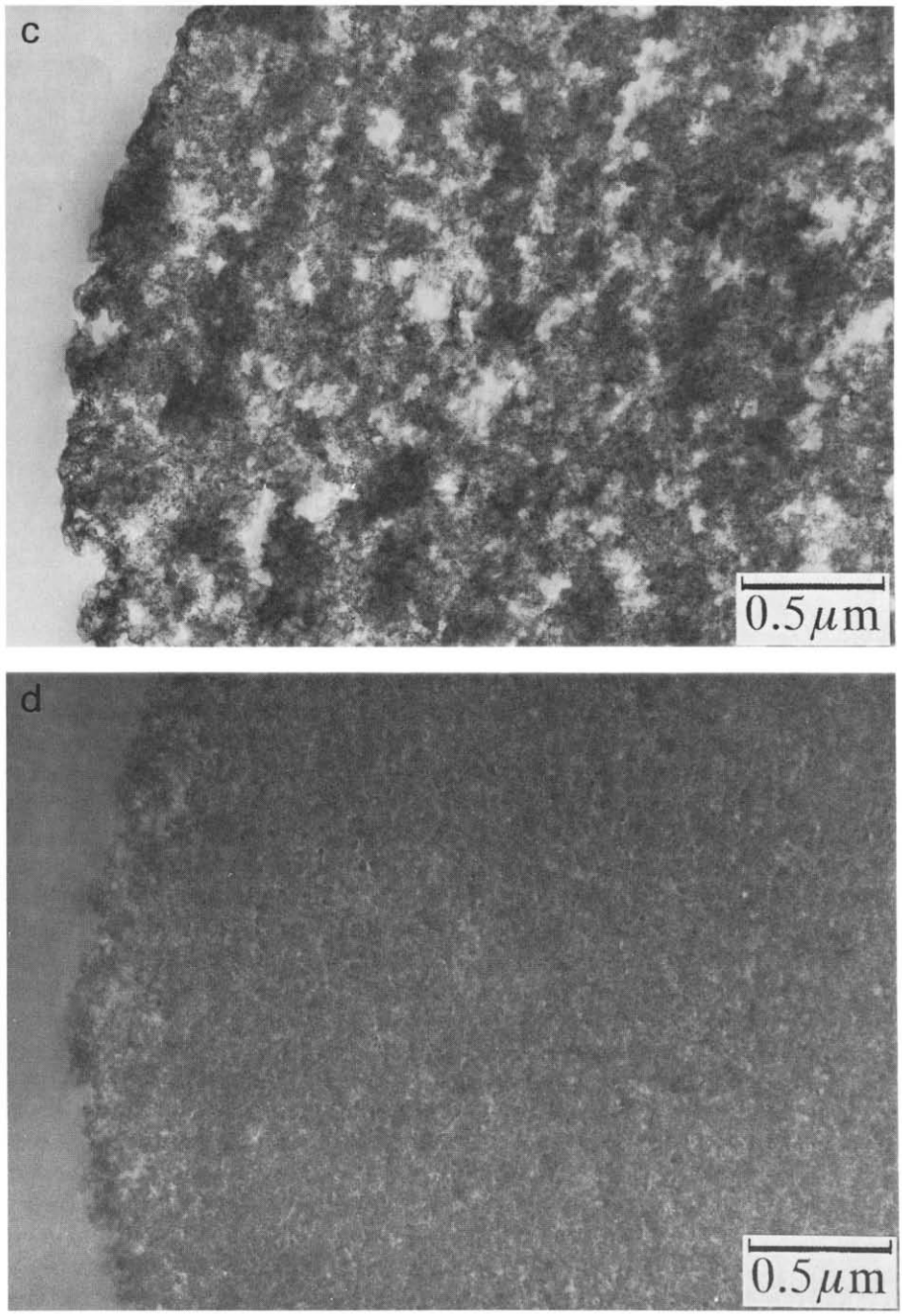

Fig. 14. TEM photographs of (a) Asahipak ODP 50, (b) PLRP-S 300, (c) Shodex D4-613 and (d) Shodex DE-613.

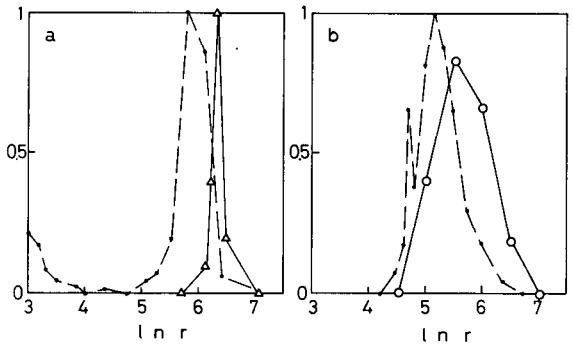

Fig. 15. Pore-size distribution of porous glass particle [(a) solid line, mercury intrusion method; dashed line, nitrogen adsorption method] and LiChrospher Si 500 [(b) dashed line, nitrogen adsorption method; solid line, inverse SEC]. The vertical axis corresponds to the fraction of pore volume, normalized in the case of inverse SEC. r = Pore radius.

6. INTERPRETATION OF RESULTS OF PORE-SIZE MEASUREMENTS BASED ON TEM OBSERVATION

Fig. 15 shows a comparison of the pore-size distributions of the glass particles and LiChrospher Si 500. As expected from the pore structures in Fig. 1, the porous glass particles gave a narrower pore-size distribution than silica particles except for the micropore range. These micropores cannot be detected by the mercury intrusion method or by TEM.

Fig. 16 shows the results of nitrogen adsorption measurements for Nucleosil 300 and Nucleosil 100. Nucleosil 300 gave a bimodal pore-size distribution, with one of the maxima at about 12 nm agreeing with that for Nucleosil 100 and the other at >50 nm. The unusual results with Nucleosil 300 are readily understandable based on particle blending shown in the TEM photographs in Fig. 6. Depending on the pore sizes and the ratio of the components, the blended particles seem to show a bimodal or broad pore-size distribution.

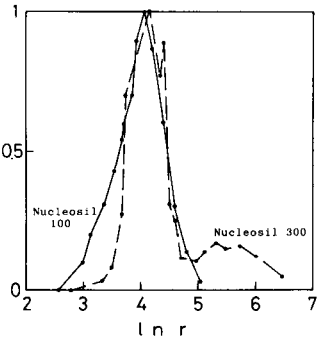

Fig. 16. Pore-size distribution of Nucleosil 100 (solid line) and 300 (dashed line) measured by nitrogen adsorption. r = Pore radius.

The SEC calibration graph obtained with standard polystyrenes in tetrahydrofuran for Nucleosil 300 indicates an extremely broad range of selective permeation from molecular weights less than 10^3 to nearly 10^6, as shown in Fig. 17. Other Nucleosil particles or LiChrospher Si 500 showed ranges of selective permeation within a factor of 100, similarly to the usual packing materials [27].

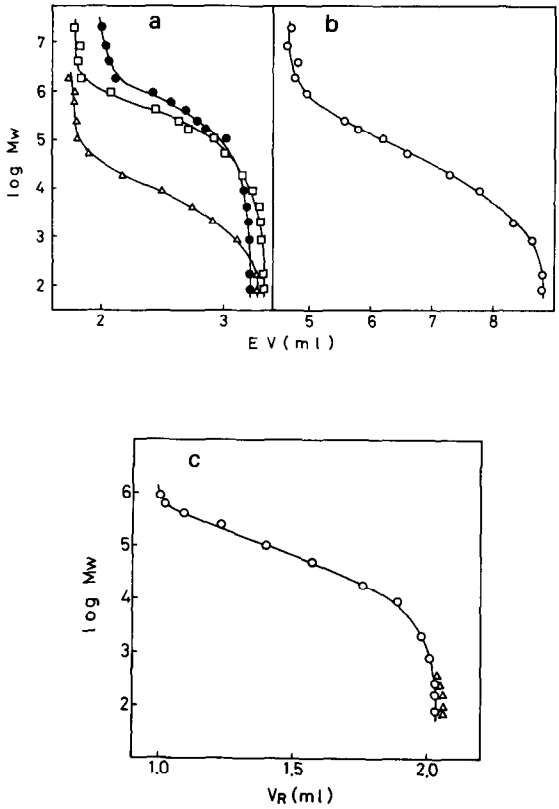

Fig. 17. Molecular weight–elution volume curves obtained on (a) Nucleosil 100 (△), 1000 (□) and 4000 (●), (b) Nucleosil 300 (○) and (c) LiChrospher Si 500. Column size: 25 cm × 4.6 mm I.D. for Nucleosil 100, 1000 and 4000, 25 cm × 8 mm I.D. for Nucleosil 300 and 15 cm × 4.6 mm I.D. for LiChrospher Si 500. Polystyrene standards were eluted with tetrahydrofuran. Alkanes (△) were also eluted in (c).

The blended particles provide a wide linear portion on the molecular weight–elution volume curve. This is in a sense a desirable feature in a packing material for SEC. The purpose of particle blending is to obtain a wide range of selective permeation in SEC and the adjustment of the surface area and the pore-size distribution within a certain specification for each batch of commercial products.

The conventional methods for the characterization of porous particles such as nitrogen adsorption and SEC give pore-size distribution data for a batch of particles. The results presented here suggest that TEM and other conventional methods can complement each other in the characterization of wide-pore particles by providing

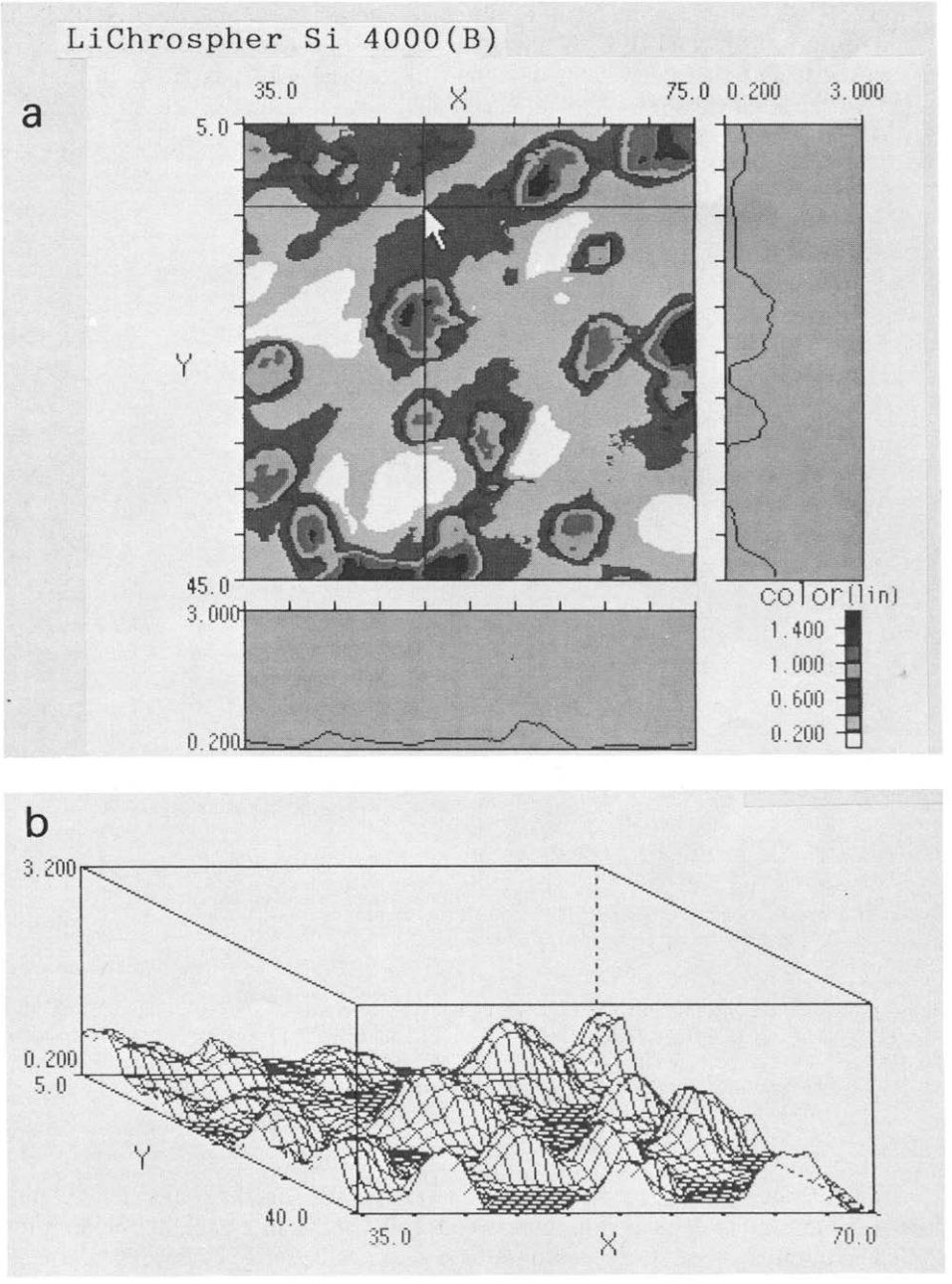

Fig. 18. Pore structure of LiChrospher Si 4000(B) expressed as (a) contour plot and (b) three-dimensional densitogram. The plots were obtained from the TEM photographs shown in Fig. 5b by scanning the areas indicated by the squares, starting from the bottom edge of the photograph, by using a densitometer. The vertical scale in (b) corresponds to the thickness of a section, *ca.* 80 nm. The densitograms at the right and bottom of the contour plot are cross-sections along the lines indicated by the arrow. The three-dimensional densitogram (b) is given for the area indicated on the axis of the contour plots (a), where the numbers represent the distance (mm) on the TEM photograph.

information on the uniformity of particles. Pore parameters in polymer and silica gels are characterized by nitrogen adsorption or by inverse SEC, whereas more specific information including the shape and the location of pores in a particle or particle blending can be obtained by TEM.

7. AN ATTEMPT TO VISUALIZE PORE STRUCTURES BASED ON TEM PHOTOGRAPHS

Several models have been proposed to provide a means of describing pore structures. These models include a simple cylindrical model and random sphere model. Knox and Scott [28] showed that the pore structures of Hypersil (*ca.* 12 nm pores) can be described by touching spheres, providing agreement between the model and the results of pore-size determination.

In the present instance, the TEM photographs of ultra-thin sections show how much of the total thickness of the section is occupied by the skeleton, and may permit the reconstruction of the original pore structures to some extent.

One can make a contour plot based on the darkness of the image on the photograph by scanning it with a light beam while measuring the reflection (a linear scan produces a densitogram as in Figs. 2 and 11). Figs. 18a and 19a were obtained from Fig. 5a and b, respectively. The squares in Fig. 5 indicate the areas scanned to produce the contour plots in Figs. 18a and 19a (note here the direction of the scan). The contour plots can be turned into three-dimensional plots (Figs. 18b and 19b, respectively), which represent the accumulation of all the material in the section on the bottom surface. The densitograms in Figs. 2 and 11 are the cross-sections of corresponding three-dimensional plots.

One has to take into account two facts with these densitograms. First, the total thickness occupied by the skeleton was projected down to the bottom surface of the ultra-thin section, and second, every face (cross-section) is expected to be equal when one plane is arbitrarily chosen from a spherical particle.

When the pores are sufficiently large, one can visualize individual structural units in the skeleton, as shown in Figs. 18 and 19. The three-dimensional densitograms show the existence of a shell at the periphery of LiChrospher Si 4000(A), and large pores up to 500 nm in LiChrospher Si 4000(B). The structures are compatible with a sphere model. Note that in Figs. 18b and 19b, the vertical scale is expanded about three times relative to the horizontal scale. It should be noted again that all the skeleton materials existing in the section are accumulated on the bottom surface. Therefore, the pore structures in Figs. 18 and 19 are not a true reconstruction of the pore structures, but they are compatible with a random sphere model, such as that given by Knox and Scott [28].

Fig. 20a shows part of a cross-section in such a touching-sphere model and a spongy system. A TEM photograph of a section including such a part would produce the densitograms shown in Fig. 20b for each arrangement of primary structures of porous materials. The complexity of the densitograms is related to the size and the numbers of spheres included in a section. One would see the similarities between Fig. 20b and the densitograms in Figs. 2, 18 and 19, taking into account the scale factor for the vertical axis.

Reconstitution of the original internal structure more realistically than in Figs. 18b and 19b may be possible by taking into account the size and shape of the primary

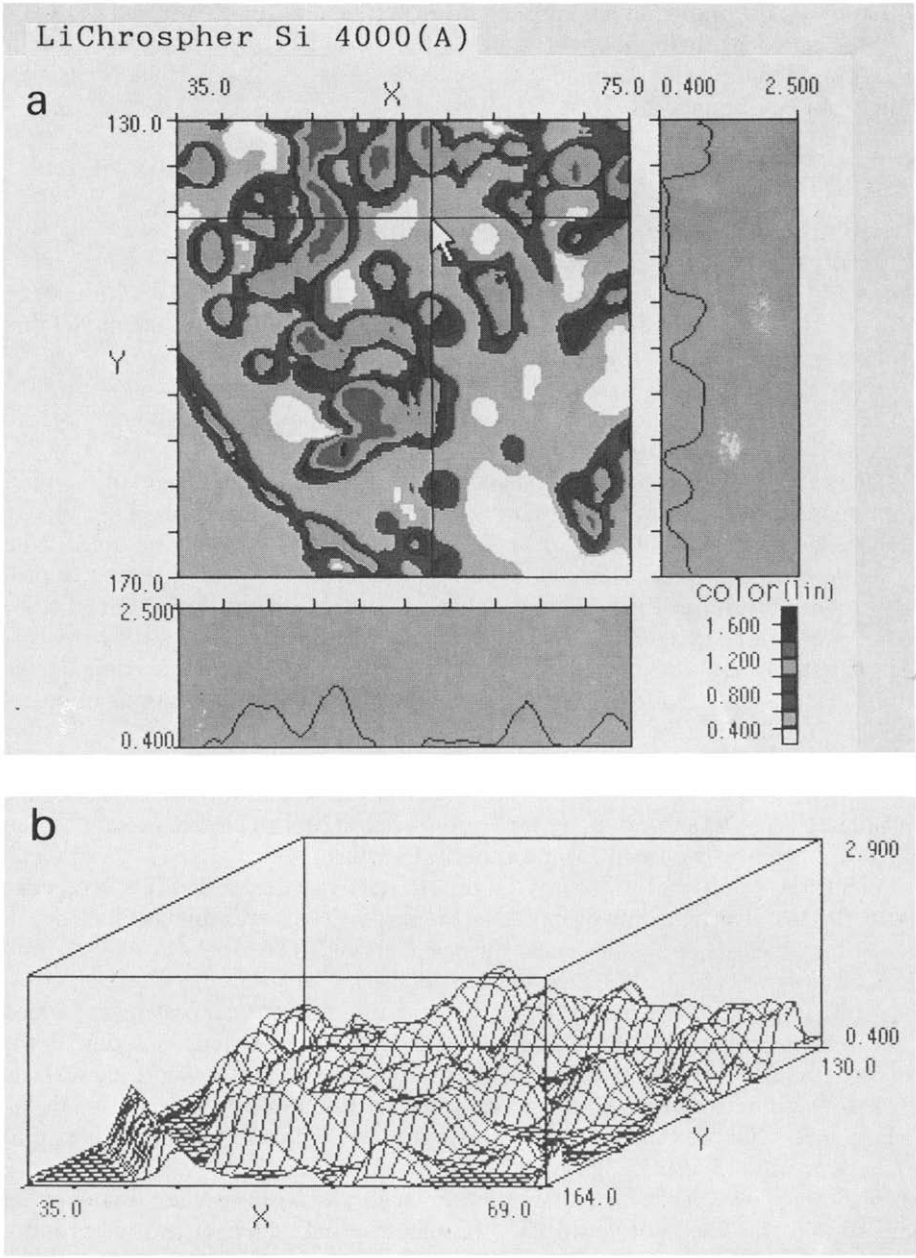

Fig. 19. Pore structure of LiChrospher Si 4000(A) expressed as (a) contour plot and (b) three-dimensional densitogram. The plots were obtained from the TEM photographs shown in Fig. 5a. Details as in Fig. 18, except for the direction of scanning, from right to left in Fig. 5a in this instance.

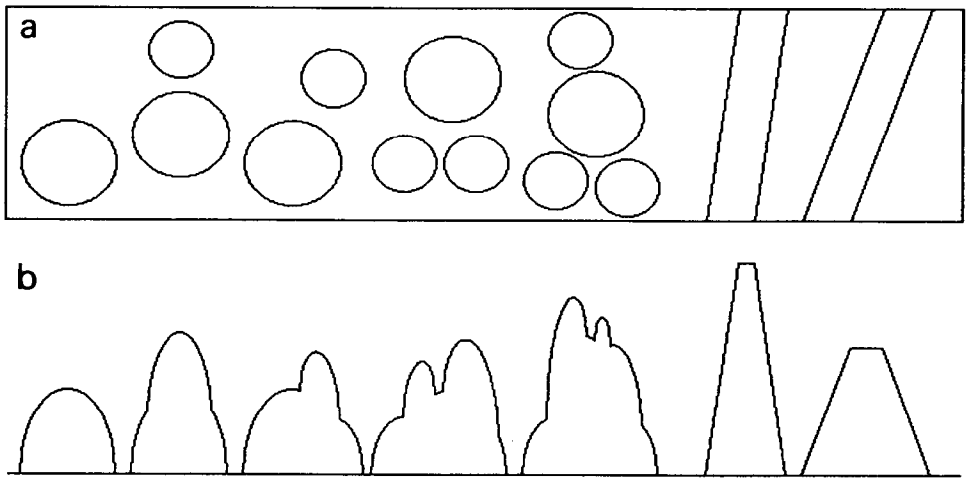

Fig. 20. (a) Several possible arrangements of touching spheres and walls in an ultra-thin section and (b) probable densitograms from imaginary TEM photographs of corresponding skeleton structure shown in (a).

structural units which appeared at the top face of the section, assuming every face is equal. The examples shown here suggest that approximate pore structures can be obtained from TEM when primary structural units are present in the section independently of each other in a highly porous system. A section of *ca.* 80 nm is thin enough to observe the internal structure of pores larger than a few hundred nanometers. With thinner sections, one can extend the study to particles with pores smaller than 100 nm.

Recent studies showed that RPLC stationary phases prepared from wide-pore silica particles, containing relatively small pores or small-pore particles in the case of blended materials, gave relatively poor results for the gradient separation of high-molecular-weight polypeptides with C_{18} derivatization [16,17]. The TEM study can help in the characterization and optimization of pore structures in these instances.

8. CONCLUSION

Clear internal structures of silica and polymer gels can be observed by TEM by preparing ultra-thin sections. TEM can provide straightforward information about the shape, location and uniformity of the pores in wide-pore packing materials for HPLC. Some of the wide-pore silicas were found to contain more than one type of particle with different internal structures. TEM complements other methods in the characterization of particles with sufficiently large pores. This study suggests the possibility of visualization of three-dimensional internal structures by using densitograms of TEM for particles having pore sizes larger than a few hundred nanometers.

9. ACKNOWLEDGEMENTS

We thank Prof. S. Hirayama of Kyoto Institute of Technology for helpful suggestions and Dr. Y. Ohtsu and Mr. Y. Shiojima of Shiseido Research Centre for

nitrogen adsorption measurements of particles. We also thank Dr. Y. Kato of Toso, Dr. I. Kaiho of Showa Denko, Dr. K. Noguchi of Asahi Chemical, Ms. L. Lloyd of Polymer Laboratories and Dr. D. Woodward of Shandon for gifts of packing materials.

REFERENCES

1 A. P. Karnaukhov, in S. Modry (Editor), *Proceedings of Rilem/IUPAC International Symposium on Pore Structure and Properties of Materials,* Vol. I, Academia, Prague, 1974, p. A-3.
2 K. K. Unger, *Porous Silica*, Elsevier, Amsterdam, 1978, Ch. 2.
3 S. D. Christian and E. E. Tucker, *Int. Lab.*, Nov./Dec. (1981) 48; Jan./Feb. (1982) 40.
4 E. Grimaud, J. C. LeCoq, E. Boschetti and M. Corgier, *J. Chromatogr.*, 166 (1978) 37.
5 R. Ruchel, R. L. Steere and E. F. Erbe, *J. Chromatogr.*, 166 (1978) 563.
6 J. Hradil, H. Horak, Z. Pelzbauer, E. Votavova, F. Svec and J. Kalal, *J. Chromatogr.*, 259 (1983) 269.
7 D. Horak, Z. Pelzbauer, F. Svec, J. Labsky and M. Bleha, *Angew. Makromol. Chem.*, 117 (1983) 117.
8 J. Hradil and F. Svec, *Angew. Makromol. Chem.*, 130 (1985) 81.
9 E. Tracz, J. Skubiszewska and R. Reboda, *J. Chromatogr.*, 287 (1984) 136.
10 E. Tracz and R. Leboda, *J. Chromatogr.*, 346 (1985) 346.
11 E. Tracz, R. Leboda and E. Mizera, *J. Chromatogr.*, 355 (1986) 412.
12 E. Tracz and A. Barna, *J. Chromatogr.*, 355 (1986) 421.
13 H. Colin and G. Guiochon, *J. Chromatogr.*, 126 (1976) 43.
14 J. H. Knox, B. Kaur and G. R. Millward, *J. Chromatogr.*, 352 (1986) 3.
15 N. Tanaka, K. Hashizume, M. Araki, H. Tsuchiya, A. Okuno, K. Iwaguchi, S. Onishi and N. Takai, *J. Chromatogr.*, 448 (1988) 95.
16 N. Tanaka, T. Ebata, K. Hosoya, T. Araki, K. Kimata, H. Tsuchiya, Y. Ohtsu and Y. Shiojima, paper presented at the *13th International Symposium on Column Liquid Chromatography, Stockholm, June 1989.*
17 N. Tanaka, K. Kimata, Y. Mikawa, K. Hosoya, T. Araki, Y. Shiojima, Y. Ohtsu, R. Tsuboi and H. Tsuchiya, *J. Chromatogr.*, 535 (1990) 13.
18 K. K. Unger and M. G. Gimpel, *J. Chromatogr.*, 180 (1979) 93.
19 J. Kohler and J. J. Kirkland, *J. Chromatogr.*, 385 (1987) 125.
20 F. Nevejans and M. Verzele, *Chromatographia*, 20 (1985) 173.
21 N. Tanaka, K. Hashizume and M. Araki, *J. Chromatogr.*, 400 (1987) 33.
22 N. Tanaka, T. Ebata, K. Hashizume, K. Hosoya and M. Araki, *J. Chromatogr.*, 475 (1989) 195.
23 N. Tanaka and M. Araki, *Adv. Chromatogr.*, 30 (1989) 81.
24 L. D. Bowers and S. Pedigo, *J. Chromatogr.*, 371 (1986) 243.
25 S. Pedigo and L. D. Bowers, *J. Chromatogr.*, 499 (1990) 279.
26 N. Tanaka, K. Kimata, K. Hosoya, T. Araki, H. Tsuchiya and K. Hashizume, *J. High Resolut. Chromatgr.*, in press.
27 L. R. Snyder and J. J. Kirkland, *Introduction to Modern Liquid Chromatography*, Wiley-Interscience, New York, 1979, Ch. 12.
28 J. H. Knox and H. P. Scott, *J. Chromatogr.*, 316 (1984) 311.